Available online at www.sciencedirect.com
SCIENCE DIRECT
Polymer 47 (2006) 3583–3590
polymer
www.elsevier.com/locate/polymer

Role of fumed silica on ion conduction and rheology in nanocomposite polymeric electrolytes

Shahzada Ahmad [a], H.B. Bohidar [b], Sharif Ahmad [c], S.A. Agnihotry [a,*]

[a] Electronic Materials Division, National Physical Laboratory, Dr K.S. Krishnan Marg, New Delhi 110012, India
[b] School of Physical Sciences, Jawaharlal Nehru University, New Delhi 110067, India
[c] Materials Research Laboratory, Department of Chemistry, Jamia Millia Islamia, New Delhi 110025, India

Received 3 May 2005; received in revised form 20 February 2006; accepted 18 March 2006

Abstract

The electrochemical, rheological, calorimetric, spectroscopic and morphological investigations have been used to examine poly(methyl methacrylate), PMMA based electrolytes dispersed with nano-sized fumed silica (SiO_2). The observed ionic conductivity was one of the highest and is of the order ~mS/cm at ambient temperature which was studied as a function of concentration of fumed silica nano-particles. It was further found that the fumed silica acted as a passive filler and played a predominant role in controlling the rheological properties while ion transport properties were least effected. The differential calorimetry studies revealed single glass transition temperature pointing towards homogeneous nature of the composite polymeric electrolytes (CPEs). At an optimum concentration of fumed silica (2 wt%) the observed maximum conductivity and morphology was attributed to the presence of a strong network structure, while at a higher concentration the elastic behavior was more pronounced which impeded ion transport. This contention was supported by spectroscopic data.

Keywords: Nanocomposite; Polymer electrolytes; Rheological properties

1. Introduction

There has been a growing interest in the utilization of alternative resources for the substitution of petroleum based products due to the exhaustion of fossil fuel stocks by the late 21st century. The emphasis has been both on the conservation and judicious usage of current resources, and on finding alternative energy sources. Much attention has been focused on the latter of these two through the development of electric vehicles, fuel cells and portable power sources largely due to the mandate driven by the government initiatives [1–4]. Lithium ion batteries constitute an important component in the techno-economic-growth and development of energy storage devices amongst many other possible electrochemical device options, due to high energy power density, low weight and excellent performance [5–7]. The addition of advanced polymer electrolytes in lithium ion batteries enhances the mechanical strength and favors gain in electrochemical properties that include manifestation of high ionic conductivity and low interfacial resistance [8,9].

Initial work on polymer electrolytes was mainly based on the complexes of poly(ethylene oxide) (PEO) with various inorganic lithium salts. These systems fail to exhibit desirable ionic conductivity due to their high degree of crystallization [10,11]. The melting of the crystalline phase of PEO around 60 °C restricts the application of electrolytes based on PEO in various electrochemical devices. Below this temperature the ionic conductivity of the polymer electrolyte is too low to warrant its practical application. To attain high ambient temperature conductivity a polymer that is amorphous in nature and has a flexible backbone is more preferred. The commonly used amorphous polymers include poly(acrylonitrile) [PAN] and poly(methylmethacrylate) [PMMA] and the high conductivity exhibited by them is due to 'gel formation', the polymer network encaging the liquid electrolyte. PAN is reported to interact more with the liquid electrolyte taking active part in the conduction mechanism, while PMMA is regarded as more passive in nature [12].

In particular, PMMA based gel electrolytes have been found to be most preferred potential candidates as electrolytes in electrochromic windows due to their high transparency as well as good gelatinizing and solvent retention ability [13,14].

* Corresponding author. Tel.: +91 11 25742610x2283; fax: +91 11 25726938.
E-mail address: agni@mail.nplindia.ernet.in (S.A. Agnihotry).

0032-3861/$ - see front matter © 2006 Published by Elsevier Ltd.
doi:10.1016/j.polymer.2006.03.059

Scrosati et al. [15] have established that the PMMA based GPEs are less reactive towards lithium electrode or are able to induce a more favorable surface. From the application point of view gel polymer electrolytes (GPEs) in addition to desirable room temperature conductivity need to have wide electrochemical potential window, and processablity and more importantly good mechanical stability. However, the conductivity and mechanical stability of GPEs are mutually exclusive, i.e. an enhancement in conductivity is achieved at the expense of reduced mechanical strength and vice versa. A novel approach to overcome the addressed shortcomings is the addition of nanosized inorganic fillers (e.g. SiO_2, Al_2O_3, TiO_2) in the GPEs to yield composite polymer electrolytes (CPEs) [16–21]. An increase in toughness can be achieved in brittle polymer through the addition of fillers such as silica particles, which have higher modulus than the matrix. The presence of fillers can give rise to flaws, which can reduce both the fracture strength of the polymer and the elongation to failure.

Fumed silica (SiO_2) is one of the best understood surfaces as far as surface chemistry is concerned. The surface chemistry of fumed silica is hydrophilic due to the presence of hydroxyl groups on the surface. Fumed silica is produced by the vapor phase hydrolysis of $SiCl_4$ in a hydrogen–oxygen flame. The word fumed silica is used due to its smoke like appearance as it forms in the flame. When immobilized in aprotic solvent, aggregates of silica can interact through H-bonding of surface hydroxyl groups, which results in formation of three-dimensional networks. In CPEs, fumed silica is not used as a catalyst but as a catalyst support instead. Lithium trifluoromethanesulfonate (LiTf), one of the several important salts is used in the preparation of liquid electrolyte in propylene carbonate (PC) in the present studies. LiTf is of choice because it is highly resistant to oxidation, thermally stable, nontoxic and insensitive to ambient moisture as compared to other lithium salts [22].

In this communication, we report, for the first time, a comprehensive understanding of the conductivity behavior of fumed silica added in different proportions to GPE prepared by PMMA immobilized liquid electrolyte comprising LiTf dissolved in PC. This has been achieved through the experimental investigations of this system through an array of techniques like calorimetry, FTIR spectroscopy, electrochemical stability analysis, and rheology that has bearing on its morphology.

2. Experimental description

2.1. Materials

Lithium trifluoromethanesulfonate, $LiCF_3SO_3$ (LiTf) salt from 3 M, PMMA (Mol. wt 996,000) of Aldrich were used after drying at 100 °C in a vacuum oven overnight. Synthesis grade propylene carbonate, PC, (Merck, Germany) was used after drying over 4 Å molecular sieves. While hydrophilic fumed silica (CABOSIL, A-200) from Cabot India Ltd was used after drying in a vacuum oven for 72 h at 120 °C.

An appropriate amount of LiTf was first dissolved in PC to result in a 1 M liquid electrolyte. The chosen concentration (1 M) in addition to the highest ionic conductivity is characterized by negligible ion pair formation in the liquid electrolyte. The fumed silica particles were then dispersed in different weight percentage under continuous stirring. After observing a homogenous mixing, 15 wt% PMMA was then added slowly while heating at 55 °C for 2 h until transparent CPEs were obtained. A total of five samples were prepared in a glove box under argon atmosphere with different concentration of fumed silica in the range (0–6 wt%) identified as CPE-2, CPE-3, CPE-4, and CPE-6, the numbers indicating the weight percent of added fumed silica in GPE.

2.2. Instrumentation

Electrolyte conductivities were measured using Metrohm 712 conductometer, controlled by a Paar Physica circulating water bath, over the temperature range 20–70 °C, after standard calibration. The conductivity cell consists of two blocking platinum wire electrodes encapsulated in a glass having a cell constant, K of 0.89 cm^{-1}. Cells are calibrated before each measurement using a standard KCl solution (1242 μS/cm at 25 °C) supplied by Metrohm.

Differential scanning calorimetry (DSC) was performed with a Mettler Toledo analyzer that consists of a DSC 851 main unit and STARe software equipped with a low temperature cell under nitrogen purge. Approximately 20 mg of samples were hermetically sealed in an aluminum pan. The samples were first annealed at 100 °C for 2 min. After that, first cooling it down to −120 °C and then retaining the samples at this temperature for 2 min, the samples were then heated to 400 °C at a rate of 10 °C/min. Glass transition temperature (T_g) and melting data were evaluated from the final heating scan. The midset of the two extrapolations was taken as T_g and the T_m was taken as the peak point of the melting endotherm. Thermogravimetric analysis (TGA) was done on Dupont TA2000 from room temperature to 450 °C at a heating of 10 °C/min in nitrogen atmosphere. Rheology measuring instrument was a stress controlled AR 500 Rheometer (TA Instruments, UK). The peltier plate on which the sample was kept had a temperature stability of ±0.1 °C. A customized solvent trap supplied by TA Instruments was used to reduce evaporation of the solvent. The measuring geometry was a 25 mm parallel plate arrangement. An equilibration time of 30 min was allowed before taking measurements for each sample. Measurements were made in the dynamic oscillation mode (strain being the controllable variable ~10%) with appropriate inertial corrections using a temperature sweep rate of 0.3 °C/min. The range of angular frequency used was from 0.5 to 100 rad/s. The temperature of all the samples was maintained at 25 °C.

Electrochemical stable potential window was determined on ECO Chemie GPES interface using two platinum electrodes and an Ag/AgCl as a reference electrode at room temperature. Infrared absorption spectra were recorded in the region of 4000–400 cm^{-1} on a computer interfaced Perkin–Elmer FX-RX1, FTIR system with a wave number resolution of 4 cm^{-1}. FTIR studies were performed at 25 °C, by sandwiching the electrolyte between KBr windows. For Raman

measurement the CPEs were placed in a glass capillary connected with a solution well at the bottom. Raman data were recorded on Perkin–Elmer GX-1 Raman 2000, in the triple subtractive mode with a CCD detector using Nd–γAg laser for excitation. The laser power used was 1500 mW, measured at the laser head with a wave number resolution of 2 cm^{-1} at 25 °C and an average of 20 scans were recorded. Scanning electron microscopy (SEM) was performed on FEI quanta 3D using a ESEM mode. The sample was mounted on a stainless steel grid, which was frozen at 2 °C under vacuum using the peltier stage due to the deformable nature of these samples.

2.3. Physical appearance

The physical appearance of the components and systems are as follows. PMMA was supplied as a white amorphous powder, while fumed silica, which is also amorphous in nature, has a three-dimensional branched chain aggregate with a length of approximately 0.2 μm with individual particle size around 15 nm. The GPE is highly transparent while the synthesized CPEs show slight loss in transparency. The measured refractive indices with the help of Abee's refractometer at 25 °C lie in the range of 1.425–1.427 for all the samples. As the loading of fumed silica increases, i.e. more than 3 wt%, it shows elastic behavior while below this content it shows viscous behavior. The CPE with 6 wt% of fumed silica is highly viscous in nature, and its conductivity is immeasurable with our current conductivity cell.

3. Results and discussion

3.1. Thermal studies

Fig. 1 shows an insight into the thermal behavior of the GPE as well as CPEs with the help of thermograms obtained by differential scanning calorimetry. The analysis of the thermogram reveals that there is a single glass transition temperature (T_g) for each CPE as well as GPE. This reflects the (i) the relatively homogeneous nature of the CPEs and (ii) their amorphous nature in the experimental temperature range from −120 to 400 °C.

It is important to note that the T_g value of PMMA (125 °C) has been lowered down enormously, by about 240 °C, in GPE with its T_g lying at −119 °C. In comparison to this, the addition of fumed silica is seen to have changed the T_g of GPE only by small values, e.g. the T_g values of CPE-2, CPE-4, and CPE-6, respectively, are −102, −104 and −106 °C. The increase rather than decrease of T_g values of CPEs with respect to GPE, though by small amount, clearly shows that the observed enhancement of the conductivity values of CPEs with reference to that of GPE is not related to the segmental motion of the polymer but to some other phenomenon, which will be discussed in detail in Section 3.3.

(Table 1) summarizes the thermal properties of the CPEs and two major endothermic peaks appear in all the thermograms in the temperature range of 230–400 °C. The one at lower temperature, which appears at 234 °C for GPE, is due to evaporation of solvent PC with its boiling point at around the same temperature. With the addition of fumed silica this peak is shifted upwards to higher temperature due to the interaction of PC with fumed silica through H-bonding. CPE-2 shows maximum shift (250.3 °C) in this temperature as compared to CPE-4 and CPE-6 loadings (243.7 and 242.56 °C). The second peak at higher temperature is at 375.3 °C for GPE and can be ascribed to degradation of unsaturated groups of PMMA [10,23,24]. It occurs at 387.5 °C in pure PMMA, the addition of fumed silica does not bring any remarkable change in this temperature, however, it shows a downward shift by 20 °C from GPE to CPEs, which in all likelihood could be due to the chemisorbed water entrapped in the polymer matrix due to the fumed silica molecule. In CPE-6, the single intense endothermic peak is replaced by multiple weak peaks extending over a wide temperature range. To further elucidate the mechanism, weight loss behavior was investigated by TGA from room temperature to 450 °C. It is evident from the Fig. 2 that the amount of residue

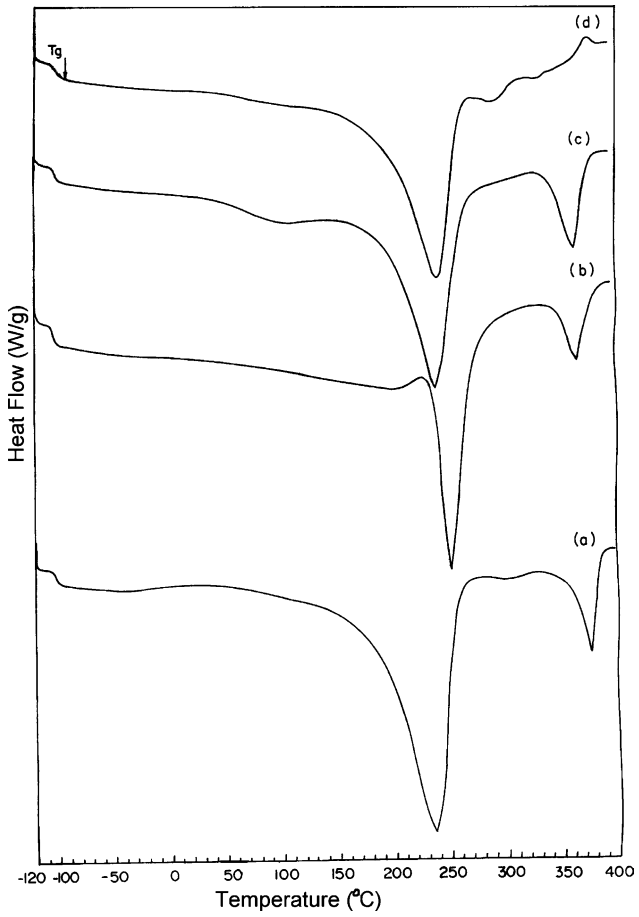

Fig. 1. DSC thermograms of (a) GPE, (b) CPE-2, (c) CPE-4 and (d) CPE-6.

Table 1
Measured thermal properties of GPE and CPEs

Sample	T_g (°C)	T_{m1}(°C)	T_{m2} (°C)
PMMA	125	275	387.5
GPE	−119.05	234	375.3
CPE-2	−102.37	250.3	365.7
CPE-4	−104.28	243.7	367.47
CPE-6	−106.91	242.5	–

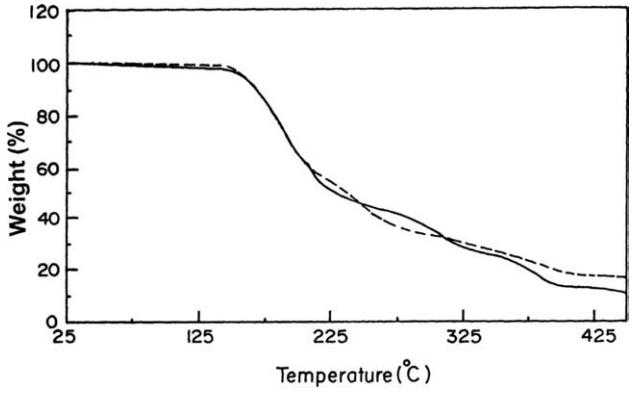

Fig. 2. TGA profiles of CPE-4 (—) and CPE-6 (– – – – –).

at 400 °C differs in the CPE-4 and CPE-6. Further, the rate of weight loss is very slow for CPE-6 than for CPE-4. This slow rate of weight loss may be corresponding to the multiple and relatively weak endothermic peaks in the DSC profile of CPE-6. Higher amount of fumed silica in CPE-6 embedded in the polymer matrix, binding the polymer more tightly, is likely to make it less volatile.

It can be thus concluded that the incorporation of fumed silica has significantly enhanced the solvent retention ability of the CPEs and has lowered T_g. This effectively widens the operational temperature range of CPEs. It is clear that fumed silica, at low loadings is more likely to coordinate with PC than with PMMA.

3.2. Rheology

Fig. 3 shows a typical plot of the elastic (G') and viscous (G'') moduli as a function of angular frequency for CPEs with different proportions of fumed silica. Both G' and G'' are frequency dependent with showing crossover. It also reflects that G' and G'' increase with fumed silica loadings.

If G' and G'' are plotted as a function of fumed silica loadings at a fixed low frequency ($\sim$1 rad/s) then at low silica

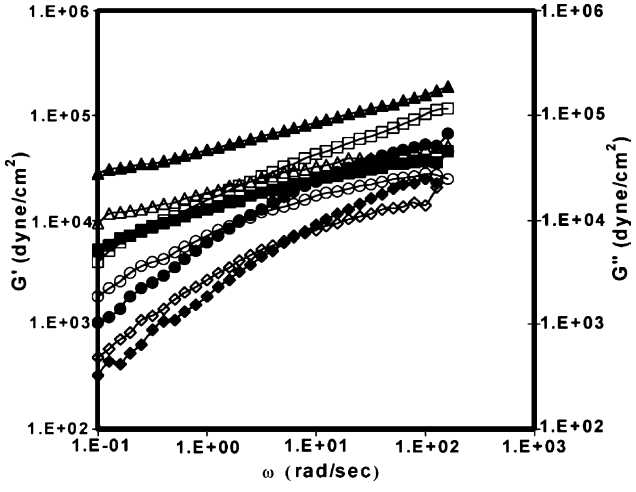

Fig. 3. Elastic (G') and viscous, (G'') moduli as a function of frequency for GPE (■), CPE-2 (●), CPE-4 (■), CPE-6 (▲). Filled symbol is for G′ and empty symbol for G″.

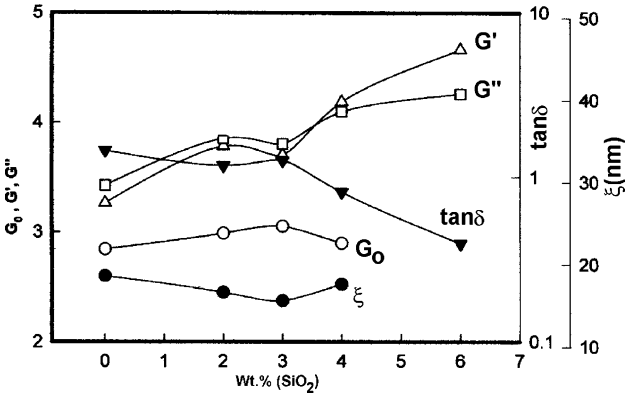

Fig. 4. $G'$and G'' at a frequency of 1 rad/s, along with the value of yield stress (G_o) and mesh size (ξ) as a function of fumed silica concentration.

loadings the viscous modulus (G'') is larger than the elastic modulus (G'), while beyond 3 wt% fumed silica, G'' becomes smaller in magnitude than G' as shown in Fig. 4.

This states the deterioration of physical association of fumed silica particle beyond 3 wt% concentration. Up to this concentration of fumed silica, content these electrolytes behave as a more viscous/liquid like, beyond that they are more elastic or solid like. The crossover of G' and G'' is taken as G_0, which is used to estimate yield stress. The three-dimensional reticulate structure formed from polymer chains and its size can be calculated depending on the strength of the bonds that form crosslinking and is called mesh size denoted by ξ and can be calculated by using following equation [25].

$$G_0 = \frac{K_B T}{\xi^3} \tag{1}$$

Where G_0 is the crossover of G' and G'', K_B is the Boltzmann constant, and T is the absolute temperature.

The network size of these systems is almost same and lies between 16 and 18 nm. There is slight attenuation in the network size from GPE to CPEs. The incorporation of fumed silica has introduced more physical linkages in the CPEs in the form of siloxane linkages, which results in a substantial increase in the gel modulus. The elastic (G') and viscous (loss) modulii (G'') were concentration (C) dependent and exhibited power law dependence with respect to filler loadings which were found to be, $G' \sim C^{n'}$, $n' = 2.7$ and $G'' \sim C^{n''}$, $n'' = 1.1$, respectively. These results demonstrate that the addition of fumed silica can induce controllable changes in the rheological properties in composite polymer electrolytes.

The data in Fig. 3 can be used to evaluate the frequency dependence of the storage and loss modulii, $G' \sim \omega^{\Delta'}$ and $G'' \sim \omega^{\Delta''}$ and terminal relaxation time τ_c as a function of fumed silica concentration. The low frequency values of Δ' and Δ'' were found to be 0.51 and 0.37, respectively, for the GPE. For CPE-6 sample the values for Δ' and Δ'' were found to be in the close proximity of each other (0.26 and 0.22, respectively) satisfying Kramer–Kronig condition. The values of these exponents decreased systematically from a maximum of $\Delta' = 0.51$ (GPE) to 0.26 (CPE-6). Similarly from $\Delta'' = 0.37$ (GPE) to 0.22 (CPE-6). This indicates growth towards an

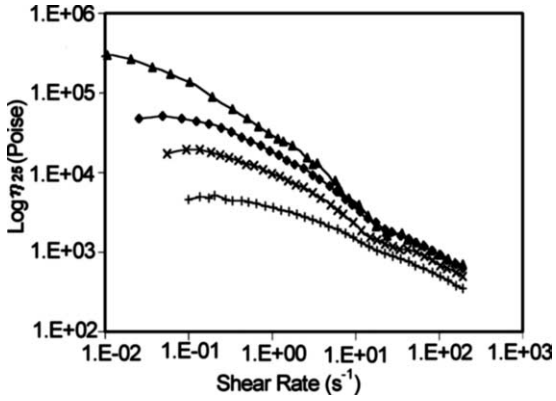

Fig. 5. Shear viscosity as a function of shear rate for GPE (+), CPE-2 (×), CPE-4 (♦) and CPE-6 (▲).

elastic solid. The values of the corresponding terminal relaxation time τ_c, ($\tau_c = 2\pi/\omega_c$, ω_c is the crossover frequency) corroborated this contention. The value of τ_c was 1 s for GPE and it increased to 25 s for CPE-4 sample. This abrupt increase in relaxation time for CPE-4 implies a more elastic or solid like structural morphology of sample CPE-4. For sample CPE-6, G' and G' do not cross each other in the experimental frequency range, i.e. its relaxation time is on the higher side.

Fig. 5 depicts shear viscosity as a function of shear rate for different concentration of fumed silica, to understand its shear thinning behavior. The viscosity shows dependence on the shear rate, without showing a linear relationship. Raghvan et al. too have established [26] that in hydrophilic fumed silica G' and G'' modulus are frequency dependent.

This frequency dependence response is characteristic of a non-flocculated dispersion in which the particulate units are distinct and separated from one another. The shear viscosity of these CPEs increased monotonically with fumed silica loadings while shear thinning behavior can only be observed at low shear rate. The viscosity decreases dramatically with increasing shear rate, this implies that the network structures are comprised of weak physical bonds, which can be disturbed by shear. At a very low shear rate, i.e. when the sample is not deformed with the increase in fumed silica loadings the viscosity changes by an order while at higher shear rate the values are comparable. The viscosity of the GPE shows less dependence on the shear rate. The presence of siloxane linkage and lack of complete relaxation chains contribute to the solid like response at low shear rates which gives rise in viscosity.

Fig. 6 depicts the thixotropic behavior of CPEs. It is well known that fumed silica forms three-dimensional network structures, which increases the viscosity of the system and produces thixotropic behavior because the shear forces from mixing are able to break the interaggregate hydrogen bonds. Thixotropic measurements probe the disruption and reformation dynamics of these networks under applied shear. In other words, a thixotropic system is one that exhibits time dependent decreasing viscosity or shear stress at a constant shear rate. The thixotropic nature of CPEs is seen to increase as the weight percent of fumed silica increases. Thixotropic behavior is desirable in various applications. At very high shear rate they

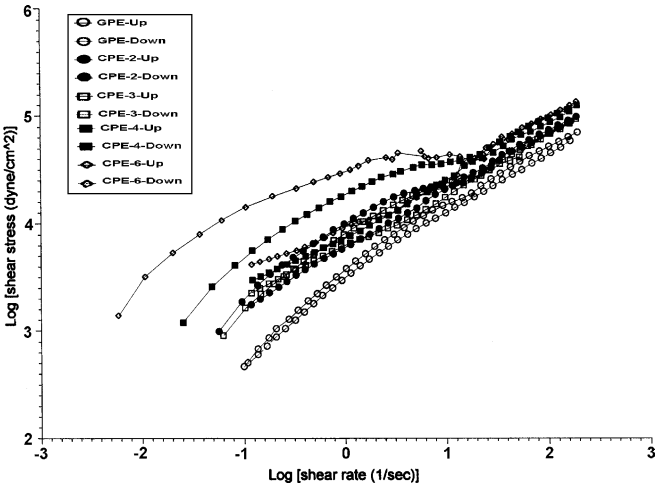

Fig. 6. Thixotropic behaviors of GPE and CPEs at 25 °C.

do not exhibit thixotropic behavior, because at this shear rate the three-dimensional network structure gets completely ruptured inelastically.

3.3. Conductivity

Fig. 7 illustrates the plots of conductivity of GPE and CPEs as a function of weight percent of fumed silica at different temperatures. Unlike systematic decrease in conductivity generally observed on polymer addition, the fumed silica addition has shown that the changes in conductivity are much smaller in comparison to those brought about by polymer addition. Additionally the changes are rather asymmetric, e.g. for CPE-2 the conductivity has increased. However, this increase in conductivity is temperature dependent, increasing with the increase of temperature. At higher loadings of fumed silica beyond 3 wt% there is decrease in conductivity that is also temperature dependent. At still higher fumed silica loadings, i.e. CPE-4 the trend is reversed but the conductivity increment relative to GPE is just by a small amount.

The maximum conductivity for CPE-2 has been realized [27] in terms of coordination of PC with fumed silica than the rest of the system, which is the strongest for CPE-2. This has also been explained due to 'electroosmotic phenomenon' by other authors [10,28]. According to them the much higher

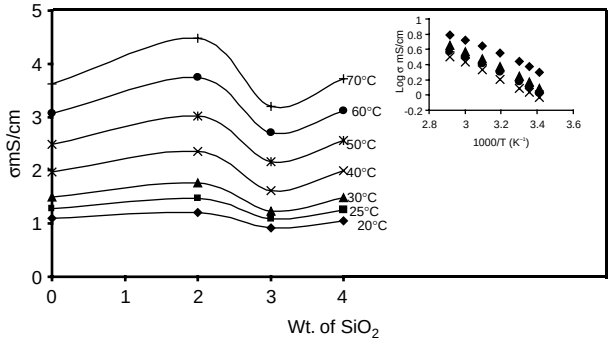

Fig. 7. Conductivity as a function of fumed silica content, inset showing Arrhenius plots of conductivity (the uppermost curve for CPE-2).

dielectric constant (64.4) of PC in comparison with that of fumed silica (4.1) is responsible for the formation of conductive region, giving more free path to Li^+ ions. Networking between PC and fumed silica in all likely hood can also encage the anions, offering free paths to Li^+ ions. The inset in Fig. 7 illustrates the Arrhenius plots for liquid electrolyte, GPE and CPEs, which shows that the maximum conductivity is exhibited by the liquid electrolyte (1 M $LiCF_3SO_3$ in PC) followed by CPE-2, GPE and CPE-4 sequentially. The profiles show more dependence of the liquid electrolyte conductivity on temperature. Arrhenius plots of log conductivity (inset of Fig. 7) are not completely linear, and show non-Arrhenius behavior characteristic of amorphous materials. Also shown are the higher conductivity changes by polymer addition than by the fumed silica addition, indicating thereby that it does not impede the mobility of Li^+ ions in the polymer electrolyte. This union of solid likes appearance and liquid like conductivity of CPEs makes polymer electrolytes so fascinating, technologically and scientifically.

3.4. Electrochemical stability

The electrochemical stability of a typical CPE with 2 wt% of fumed silica is shown in Fig. 8. CPE with 2 wt% of fumed silica is chosen due to its superior characteristics among other CPEs. The figure depicts the cyclic voltammogram measured between ± 5.0 V on platinum electrodes at a scan rate of 20 mV/s. The result exhibits a stable potential range upto $\pm$ 4.0 V. The excessive increase of current at ± 4.0 V is the indication of crossing the safe value of the voltage.

3.5. Spectral studies

Understanding of the possible interactions between various components of GPE and CPEs and their effect on the properties of the electrolyte can be obtained from the FTIR and Raman spectra, of particular interest is to probe the possible changes responsible for the increase in conductivity for CPE-2. As discussed earlier the enhancement in the mobility of the charge carriers due to decrease of T_g making the polymer chains more flexible appears to be unlikely. Alternatively either the charge carrier concentration increase could be possible reason or some changes in the local distribution of the components/trapping of the anions after the addition of fumed silica making the path of Li^+ ions more free could lead to the observed increased conductivity. In order to probe this both FTIR and Raman spectra of GPE and CPE-2 were examined.

It may first be brought to the notice that the addition of fumed silica does not show its characteristic bands in the spectra (either Raman or FTIR) possibly because the size is so small that it just disrupts the initial order in the polymer matrix. However, the local structural changes may take place, which are conducive for conductivity increase. Indeed changes observed in the spectra are good indicators of the same, which are discussed below.

Some changes are observed in the region where the characteristic bands of the anions generally lie, e.g. in the region from 1030 to 1060 cm^{-1}. This is the region corresponding to the bands (1) the non-degenerate vibrational mode of ν_s (SO_3) appearing at 1030–1034 cm^{-1} coming from the free triflate anions (2) the 1040–1045 cm^{-1} absorption from the monodendate ion-paired triflate and (3) the 1049–1053 cm^{-1} band from the more highly aggregated triflates [29,30]. Raman band at 1032 cm^{-1} in the spectrum of GPE (Fig. 9) has been found to be unperturbed pointing towards no change in the free triflate anions. In contrast the FTIR band at 1052.5 cm^{-1} corresponding to highly aggregated triflate anions has exhibited a downward shift to 1050.2 cm^{-1}.

The region of ν_{as} (SO_3) located at 1200–1320 is unaffected by the addition of fumed silica. Noticeable changes are seen in the region where distinct bands due to symmetric deformation δ_s (CF_3) occur due to differently associated ionic species. Free ions and the aggregate species, respectively, give bands in the frequency regions 756–758 and 761–763 cm^{-1} [28,31]. A Raman band appearing at 757 cm^{-1} in the spectrum of GPE is shifted to 759.5 cm^{-1} with the addition of fumed silica in CPE-2.

Another noticeable change observable is in the region, which shows signature of Li^+– PMMA interaction [11]. The band due to O=C–O bending mode appears at 817 cm^{-1} in the

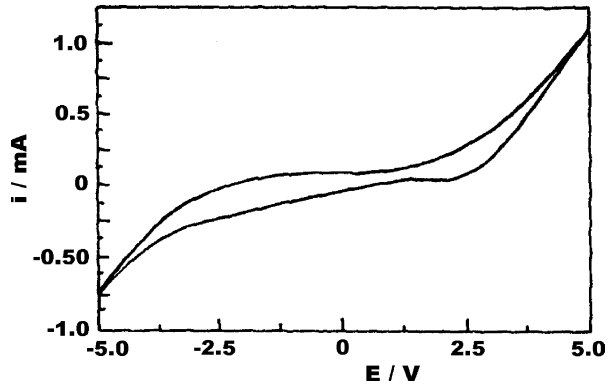

Fig. 8. Cyclic voltammogram of CPE-2 at a scan rate of 20 mV/min.

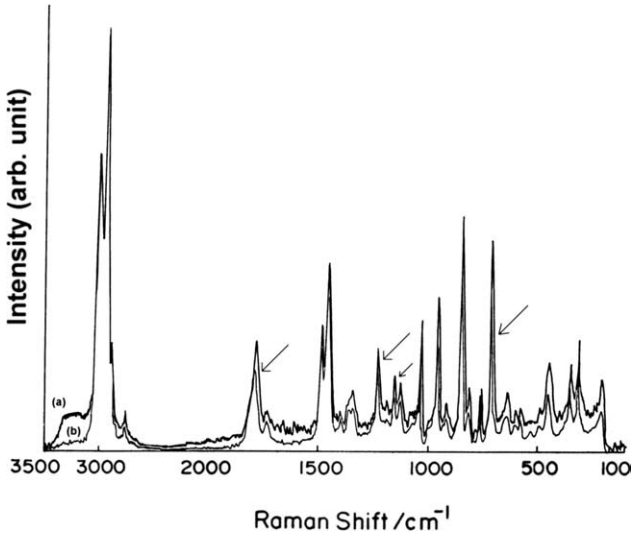

Fig. 9. Raman spectra of (a) GPE and (b) CPE-2.

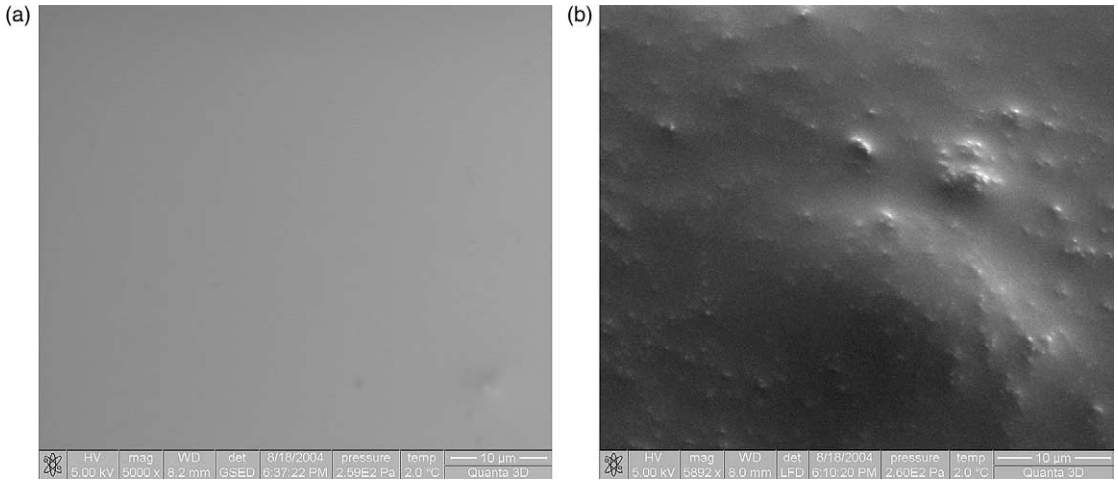

Fig. 10. ESEM of (a) GPE (b) CPE-2.

Raman spectrum of CPE-2. The induction of fumed silica making the coordination loose may be responsible for this observed change. Additional source of information is with reference to bands occurring at 1117, 1339–1354 cm^{-1} due, respectively, to ρ_w(C–H) + δ(C–H) and vibrational modes of PC show evident changes as shown in the spectra.

Although the observed shifts are on a small scale these are the positive indications of local structural changes induced by the addition of fumed silica making the path for Li^+ ions more free with their transport becoming faster/easy and as a result increasing the conductivity.

3.6. Morphology

Scanning electron micrographs of the GPE and CPE-2 reveal large difference in surface morphology. Since, both the polymer and fillers are amorphous in nature, so there are no crystalline domains but spherulitic structures are evident. The GPE shows homogenous surface morphology.

Individual fumed silica particles appear to form a highly branched morphology possessing high interfacial area. It is obvious from the Fig. 10(b) that fumed silica is mostly dispersed as small aggregates and even of individual particles. Many of this individual particles measure 0.2 μm, while the aggregates measure 2.5 μm, the spacing between the particles are not uniform.

4. Conclusion

In this study, CPEs have been synthesized by dispersing fumed silica (SiO_2) maximum upto 6 wt%, into a matrix formed by lithium triflate in an aprotic solvent propylene carbonate (PC) and the polymer PMMA. These new types of CPEs are homogeneous with high ionic conductivity, wide electrochemical stability and in particular excellent rheological properties at ambient temperature. Further, the thermal stability along with shear thermal behavior advantageous for the fabrication of advanced electrochemical devices. The addition of fumed silica, due to its hydrophilic nature form an open network structure that provides relatively unimpeded movement of the Li^+ ions. The network structure imparts mechanical stability to the CPEs and according to the requirements of specific applications the rheological properties can be tailored by varying the fumed silica content without significantly affecting the ion transport. FTIR and Raman spectroscopic investigations also support local structural changes induced by the addition of fumed silica making the path for Li^+ ions more free encaging the anions in the matrix.

Our concluding remark from the present studies is that the fumed silica is passive filler in the CPEs. The mechanical properties of such CPEs are primarily governed by the fumed silica whereas ion transport is dictated by the pristine GPE.

Acknowledgements

The authors express their gratitude to the Ministry of Non-Conventional Energy Sources, India for the financial support of this work. One of us Shahzada Ahmad acknowledges CSIR for a senior research fellowship. Thanks are also due to Dr S.K. Dhawan for DSC measurements and Somak Chatterjee for his assistance with rheological measurements.

References

[1] Florjanczyk Z, Monikowska EZ, Wieczorek W, Ryszawy A, Tomaszewska A, Fredman K, et al. J Phys Chem B 2004;108:14907–14.
[2] Singhal RG, Capracotta MD, Martin JD, Khan SA, Fedkiw PS. J Power Sources 2004;128:247–55.
[3] Song JY, Wang YY, Wan CC. J Power Sources 1999;77:183–97.
[4] Swierczynski D, Zalewska A, Wieczorek W. Chem Mater 2001;13:1560–4.
[5] Abraham KM, Jianz Z, Carroll B. Chem Mater 1997;9:1978–88.
[6] Walls HJ, Riley MW, Singhal RR, Spontak RJ, Fedkiw PS, Khan SA. Adv Funct Mater 2003;13:710–7.
[7] Karlinsey RL, Bronstein LM, Zwanziger JW. J Phys Chem B 2004;108:918–28.
[8] Bohnke O, Rousselot C, Gillet PA, Truche C. J Electrochem Soc 1992;139:1862–5.

[9] Appetechi GB, Croce F, Romagnoli P, Scrosati B, Heider U, Oesten R. Electrohem Commun 1999;1:83–6.
[10] Meneghetti P, Quatubuddin S, Webber S. Electrochim Acta 2004;49: 4923–31.
[11] Ahmad S, Ahmad S, Agnihotry SA. J Power Sources 2005;140:151–6.
[12] Johansson P, Edvardsson M, Adebahr J, Jacobsson P. J Phys Chem B 2003;107:12622–7.
[13] Deepa M, Agnihotry SA, Gupta D, Chandra R. Electrochim Acta 2004; 49:373–83.
[14] Agnihotry SA, Ahmad S, Gupta D, Ahmad S. Electrochim Acta 2004;49: 2343–9.
[15] Appetechi GB, Croce F, Scrosati B. Electrochim Acta 1995;40:991–7.
[16] Walls HJ, Fedkiw PS, Zawodzinsky Jr TA, Khan SA. J Electrochem Soc 2003;150:E165–E74.
[17] Croce F, Appetechi GB, Persi L, Scrosati B. Nature 1998;394:456–8.
[18] Appetechi GB, Romagnoli P, Scrosati B. Electrohem Commun 2001;3: 281–4.
[19] Kumar B. J Power Sources 2004;135:215–31.
[20] Adehar J, Byrne N, Forsyth M, MacFarlane DR, Jacobsson P. Electrochim Acta 2003;48:2099–103.
[21] Johansson P, Jacobsson P. Solid State Ionics 2004;170:73–8.
[22] Webber A. J Electrochem Soc 1991;138:2586–96.
[23] Grillone AM, Panero S, Retamal BA, Scrosati B. J Electrochem Soc 1999; 146:27–31.
[24] Aymonier C, Bortzmeyer D, Thomann R, Mulhaupt R. Chem Mater 2003; 15:4874–8.
[25] Abdellah A, Choplin L. Macromolecules 1991;24:5221–3.
[26] Raghavan SR, Riley MW, Fedkiw PS, Khan SA. Chem Mater 1998;10: 244–51.
[27] Fan J, Fedkiw PS. J Electrochem Soc 1997;144:399–408.
[28] Fritz HP, Stein K, Herr R. J Power Sources 1992;37:315–23.
[29] Huang W, Frech R, Wheeler RA. J Phys Chem 1994;68:100–10.
[30] Kim CS, Oh SM. J Power Sources 2002;109:98–104.
[31] Kakihana M, Schantz S, Torell LM. J Chem Phys 1990;92:6271–7.